

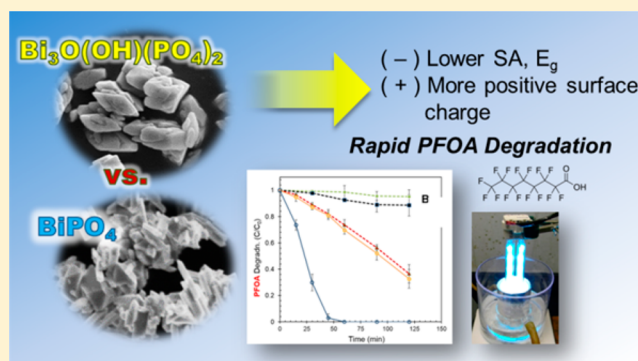
# Rapid Degradation and Mineralization of Perfluorooctanoic Acid by a New Petitjeanite $\text{Bi}_3\text{O}(\text{OH})(\text{PO}_4)_2$ Microparticle Ultraviolet Photocatalyst

Sushant P. Sahu, Mojtaba Qanbarzadeh, Mohamed Ateia,<sup>1</sup> Hamed Torkzadeh, Amith S. Maroli, and Ezra L. Cates\*<sup>2</sup>

Department of Environmental Engineering and Earth Sciences, Clemson University, Clemson, South Carolina 29634, United States

## Supporting Information

**ABSTRACT:** Water treatment techniques for destructive removal of perfluoroalkyl substances (PFAS) have only recently begun to emerge in the research literature, comprising unconventional advanced oxidation and reduction methods. Photocatalytic degradation of PFAS has not been widely pursued, which is a result of the limited ability of common semiconductor materials to induce C–F bond cleavage in aqueous systems. Herein, degradation of perfluorooctanoic acid (PFOA) by bismuth phosphate photocatalysts under ultraviolet irradiation has been investigated for the first time, including the relatively well-known monoclinic  $\text{BiPO}_4$  wide band gap semiconductor, as well as a novel  $\text{Bi}_3\text{O}(\text{OH})(\text{PO}_4)_2$  (BOHP) composition. Compared to  $\text{BiPO}_4$  and a  $\beta\text{-Ga}_2\text{O}_3$  nanomaterial reference catalyst, BOHP microparticles achieved dramatically faster PFOA degradation and mineralization, despite both a smaller surface area and a lower band gap energy. The rate constant for degradation of PFOA by BOHP in a pure water solution was  $\sim 15$  times greater than those of both  $\text{BiPO}_4$  and  $\beta\text{-Ga}_2\text{O}_3$  ( $\sim 20\text{--}30$  times greater when normalized for surface area) and was on the same order of magnitude as that of phenol degradation by P25  $\text{TiO}_2$  in the same photoreactor. The superior performance of BOHP was primarily related to the surface charge and adsorption behavior of PFOA, in combination with the favorable redox potentials of BOHP charge carriers. The catalyst was further tested at low PFOA concentrations (i.e., microgram per liter range) in the presence of natural organic matter, and rapid degradation of PFOA was also observed, indicating the potential of BOHP to enable practical ex situ destructive treatment of PFAS-contaminated groundwater.



## INTRODUCTION

Cost-effective treatment options for poly- and perfluoroalkyl substances (PFAS), an emerging class of highly recalcitrant water contaminants, have yet to be established. The continuing proliferation of PFAS in consumer products and firefighting foams and subsequent accidental releases into the environment are adding urgency to this challenge.<sup>1–3</sup> Moreover, recent research has found that optimizations of more conventional treatment operations to target PFAS are often insufficient or require further disposal.<sup>4,5</sup> Advanced oxidation and reduction processes shown to fully degrade PFAS thus far include ultraviolet (UV)/sulfite (reduction)<sup>6,7</sup> and electrochemical techniques,<sup>8,9</sup> both in early stages of development. Photocatalytic degradation has been largely discounted as a useful weapon against PFAS, as the practical  $\text{TiO}_2$  nanoparticle catalysts show low activity against fluorinated organics because of insufficient redox potential.<sup>10–12</sup> While commercial  $\text{TiO}_2$ -based slurry photocatalytic systems have proven to be successful in groundwater pump-and-treat operations for other synthetic organic contaminants,<sup>13</sup> few catalytic materials are known to have significant photocatalytic activity against

PFAS. Most notably, Shao et al. demonstrated complete degradation of perfluorooctanoic acid (PFOA) by “sheaf-like”  $\beta\text{-Ga}_2\text{O}_3$  nanomaterials in  $\sim 45$  min under UVC irradiation (254 nm, pH 4.7).<sup>14</sup> The high conduction band edge potential of  $\beta\text{-Ga}_2\text{O}_3$  of  $-1.55$  eV (vs the normal hydrogen electrode)<sup>15</sup> allows direct heterogeneous reaction of perfluorocarboxylic acids with photoexcited semiconductor electrons ( $e_{\text{cb}}^-$ ).<sup>11</sup> Huang et al. even reported reductive degradation of the much more recalcitrant perfluorooctanesulfonic acid by a SiC photocatalyst, though the rate was prohibitively slow ( $k_{\text{first order}} = 0.098 \text{ h}^{-1}$ ).<sup>16</sup>

Herein, we examine the photocatalytic activities of bismuth phosphate semiconductor materials for PFOA degradation, including  $\text{BiPO}_4$  and  $\text{Bi}_3\text{O}(\text{OH})(\text{PO}_4)_2$  [bismuth oxyhydroxyphosphate (BOHP)]. Pan et al. first reported the photocatalytic activity of  $\text{BiPO}_4$  submicrometer particles in 2010,

Received: July 30, 2018

Revised: July 31, 2018

Accepted: August 1, 2018

Published: August 1, 2018

which outperformed P25 TiO<sub>2</sub> with respect to degradation of model wastewater contaminants under UVC irradiation (e.g., phenol and methylene blue).<sup>17,18</sup> Among the three known BiPO<sub>4</sub> polymorphs, including one hexagonal (h-BiPO<sub>4</sub>) and two monoclinic (m-BiPO<sub>4</sub> and n-BiPO<sub>4</sub>) phases, n-BiPO<sub>4</sub> is now established as the most photocatalytically active.<sup>18–20</sup> Its superiority has been attributed to distortion of PO<sub>4</sub><sup>3–</sup> tetrahedra in this structure, creating a greater dipole moment that more strongly attracts valence band holes (h<sub>vb</sub><sup>+</sup>) and prolongs the charge carrier lifetime.<sup>19</sup> Unlike BiPO<sub>4</sub>, BOHP has not been studied with respect to photocatalytic processes or, to the best of our knowledge, any other application. Its existence in the literature is restricted to a mineralogical finding in Germany, wherein the material was found to be a triclinic structure of space group P1̄ and given the name Petitjeanite.<sup>21</sup> Degradation of fluorinated compounds by bismuth phosphates has not been reported to the best of our knowledge; however, the exceptional electron–hole separation and high band gap energies ( $E_g$ , 3.5–4.6 eV)<sup>20</sup> typical of these materials were hypothesized to be conducive to PFAS activity.

## MATERIALS AND METHODS

Reactant chemical sources and purities are described in Text S1, and characterization and analytical methods in Text S2. BOHP, BiPO<sub>4</sub>, and β-Ga<sub>2</sub>O<sub>3</sub> were synthesized via hydrothermal methods using Teflon-lined stainless steel autoclaves, as described in Text S3. The BOHP material was formed by modifying the n-BiPO<sub>4</sub> synthesis of Pan et al.<sup>17</sup> by changing the reaction pH from 1 to 10 with NH<sub>4</sub>OH.

Photocatalytic treatments were conducted in a 280 mL cylindrical fused silica reactor vessel equipped with external anodized aluminum reflective jacket and magnetic stirring and partially submerged in a flowing water bath to maintain room-temperature conditions. An 18 W compact fluorescent low-pressure Hg lamp (254 nm) was submerged in the reactor in a pseudoannular configuration, with a lamp-to-wall distance of approximately 2 cm. Additional details, including information about natural organic matter (NOM) addition, catalyst reusability tests, and adsorption experiments, are provided in Texts S4–S6.

## RESULTS AND DISCUSSION

X-ray diffraction data for BiPO<sub>4</sub> particles are shown in Figures S1A, and scanning electron microscopy (SEM) results can be found in our previous work.<sup>22</sup> Results were consistent with those of Pan et al., with hydrothermal treatment at pH 1 resulting in mainly ~1 μm elongated crystals of the n-BiPO<sub>4</sub> monoclinic structure (hereafter simply termed BiPO<sub>4</sub>).<sup>17</sup> Results of energy-dispersive X-ray spectroscopy (EDS) analyses (Figure S2A) yielded an observed B/P/O atomic ratio of 1.0/0.9/4.0, consistent with the desired composition. As shown in Figure 1A, synthesis at an elevated pH of 10 resulted in higher-dimensional 1.5–3.0 μm long fused aggregates, with primary crystallite sizes of several hundred nanometers. The X-ray diffraction (XRD) pattern for this material (Figure 1C) matched that of BOHP, which is isostructural to the more widely reported Bi<sub>3</sub>O(OH)(AsO<sub>4</sub>)<sub>2</sub> (Preisingerite).<sup>21,23</sup> Because the concentration of OH<sup>–</sup> in the reactant solution was 9 orders of magnitude greater than that prepared at pH 1, the formation of BOHP was attributed to the greater thermodynamic driving force for incorporation of OH<sup>–</sup>/O<sup>2–</sup> during precipitation and crystallization. EDS results

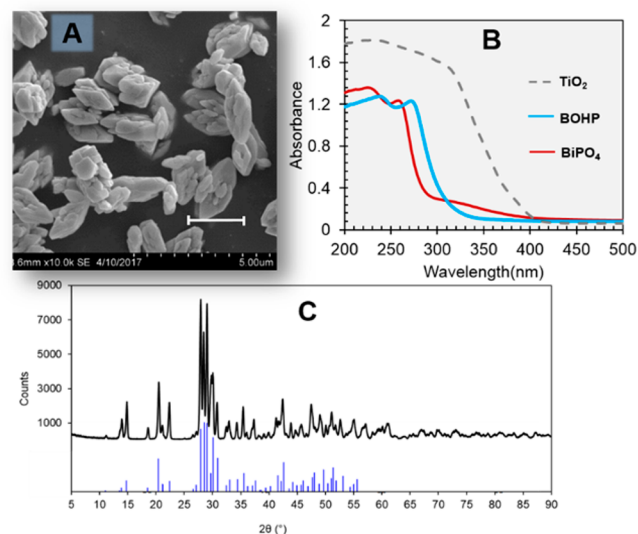


**Figure 1.** Characterization data for catalyst powder samples, including (A) a SEM image of BOHP (white bar, 2 μm), (B) diffuse-reflectance absorption spectra of BOHP and BiPO<sub>4</sub> with TiO<sub>2</sub> data included for comparison, and (C) the XRD pattern of BOHP with the Petitjeanite reference pattern (PDF 00-046-1477).

were also consistent with the established BOHP composition, indicating an average B/P/O atomic ratio of 3.0/1.8/9.8 (Figure S2B). To the best of our knowledge, this is the first report of synthetically prepared BOHP. The XRD and SEM results for the β-Ga<sub>2</sub>O<sub>3</sub> reference catalyst, shown in Figures S1B and S3, respectively, were consistent with those of Shao et al.<sup>14</sup> and showed the expected “sheaf-like” aggregated nanorod morphology. The crystallite size of our β-Ga<sub>2</sub>O<sub>3</sub> samples, despite following the same method, was considerably larger and resulted in a smaller surface area, as described below. Diffuse-reflectance spectroscopy was used to estimate the  $E_g$  of BiPO<sub>4</sub> and BOHP, with results shown in Figure 1B and Table 1. For BiPO<sub>4</sub>, the absorption spectrum indicated an  $E_g$  of 4.19 eV and also showed a shoulder peak at a lower energy, attributed by others to the presence of surface oxygen vacancies.<sup>24</sup> The observed  $E_g$  of BOHP was lower at 3.90 eV, as expected due to replacement of some PO<sub>4</sub><sup>3–</sup> oxyanion groups with O<sup>2–</sup>, which has a lower electron binding energy (the  $E_g$  of Bi<sub>2</sub>O<sub>3</sub>, for example, is 2.8 eV).<sup>25</sup> The  $E_g$  values of TiO<sub>2</sub> (anatase) and β-Ga<sub>2</sub>O<sub>3</sub> reference catalysts were 3.18 and 4.80 eV (from the literature<sup>14</sup>), respectively. According to BET analyses, surface areas of the powders decreased in the following order: 5.9 m<sup>2</sup>/g (β-Ga<sub>2</sub>O<sub>3</sub>) > 3.6 m<sup>2</sup>/g (BiPO<sub>4</sub>) > 2.5 m<sup>2</sup>/g (BOHP).

Degradation of phenol under UVC irradiation was used to gauge the general photocatalytic activities of the bismuth phosphate materials toward a simple aromatic organic contaminant, with TiO<sub>2</sub> serving as a reference catalyst. Degradation rates (Figure 2A) were observed to increase in the order photolysis (no catalyst) < TiO<sub>2</sub> < BiPO<sub>4</sub>, which mirrored the results of Pan et al. for methylene blue degradation.<sup>17</sup> The BOHP material, however, showed the lowest photocatalytic activity for phenol, with a first-order rate constant that was 10 times lower than that of BiPO<sub>4</sub>. Degradation therein was also slower than in the control experiment, because BOHP absorbed UV to prevent photolysis but yielded little photocatalytic action. The smaller surface area of this material certainly contributed to this result. Figure 2B

Table 1. Selected Properties of Bismuth Phosphate Photocatalysts and the Ga<sub>2</sub>O<sub>3</sub> Reference Catalyst<sup>a</sup>

material	form	band gap energy (eV)	BET surface area (m <sup>2</sup> /g)	PFOA <i>k</i> (h <sup>-1</sup> )	SA-normalized <i>k</i>
β-Ga <sub>2</sub> O <sub>3</sub>	sheaf-like nanomaterial	4.80	5.9	0.44	0.075
n-BiPO <sub>4</sub>	submicrometer particles	4.19	3.6	0.40	0.11
BOHP	microaggregates	3.90	2.5	6.0	2.4

<sup>a</sup>*k*, pseudo-first-order rate constant; SA, specific surface area.

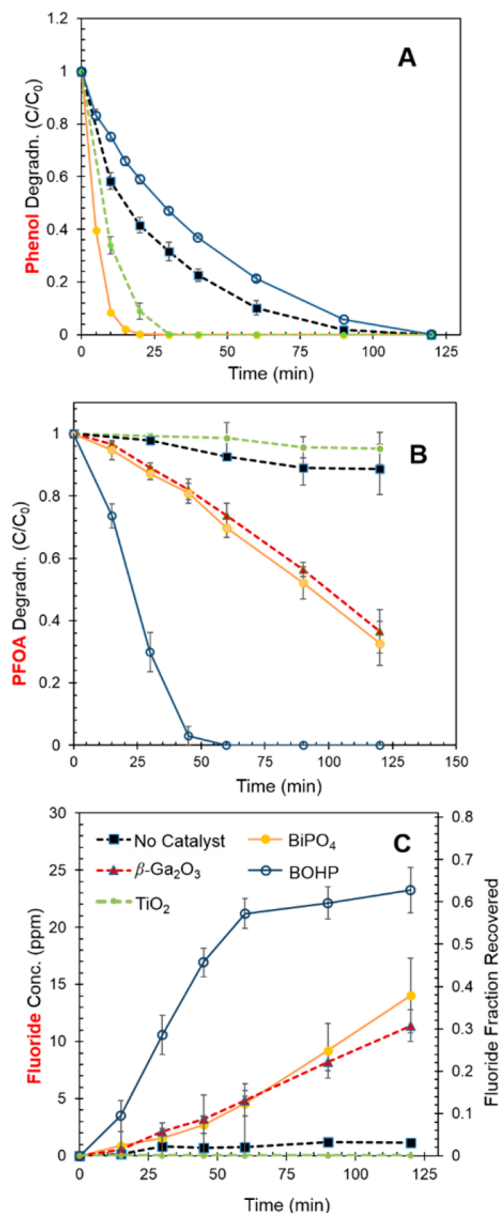


**Figure 2.** Photocatalytic degradation of contaminants by particle suspensions under UVC irradiation, including (A) phenol degradation, (B) PFOA degradation, and (C) F<sup>-</sup> liberation during PFOA degradation. The legend in panel C applies to all panels. Error bars show standard deviations of separate experiments performed in triplicate.

shows the PFOA linear isomer<sup>26</sup> degradation kinetics under an ambient atmosphere for each photocatalyst. Therein, TiO<sub>2</sub> had negligible activity against the fluorinated contaminant as expected, while BiPO<sub>4</sub> degraded PFOA as fast as the most effective previously reported UVC photocatalyst, β-Ga<sub>2</sub>O<sub>3</sub>, with ~70% removal after irradiation for 20 min. Surprisingly,

the BOHP particles resulted in much faster PFOA degradation, despite its smaller surface area and poor efficacy in degrading phenol. The pseudo-first-order PFOA degradation rate constants for BiPO<sub>4</sub>, β-Ga<sub>2</sub>O<sub>3</sub>, and BOHP were 0.40, 0.44, and 6.0 h<sup>-1</sup>, respectively. The performance of BOHP represents the highest photocatalytic activity for PFOA under ambient conditions reported to date, and in fact, the rate constant was on the same order of magnitude as that of phenol degradation by TiO<sub>2</sub> in our photoreactor (~10 h<sup>-1</sup>). Normalizing for surface area, we found the rate constants for PFOA degradation were 0.074, 0.11, and 2.4 h<sup>-1</sup> for β-Ga<sub>2</sub>O<sub>3</sub>, BiPO<sub>4</sub>, and BOHP, respectively, indicating further opportunity for performance enhancement through synthesis of smaller BOHP particles. Figure 3A shows the results of BOHP reusability tests (Text S5), indicating no significant change in PFOA degradation ability after five cycles of reuse. The greater variability of results for cycles 2–5 was due to variable aggregation of recycled catalyst particle suspensions; the surface area was thus affected, but no change in overall photocatalytic activity was evident, affirming the chemical stability of BOHP microparticles. We note that a mild rinsing procedure was used to adequately control the initial PFOA concentration at the start of each run; however, the particles were not soaked in pure water for an extended period to preserve any strongly adsorbed compounds that might accumulate during application in a real treatment system.

The mineralization of PFOA was monitored via both TOC reduction (Figure S4) and fluoride ion liberation (Figure 2C). For both data sets, the relative kinetics were of the same ranking as with degradation, with BOHP showing significantly faster mineralization. With respect to TOC, mineralization plateaued at ~84% removal (relative to initial experimental TOC concentrations), which indicated possible generation of an organic intermediate compound(s) that was more resistant to photocatalytic degradation. A mass balance on fluorine atoms also supported this assertion, with 63% of fluorine recovered as F<sup>-</sup> in solution. Volatilization of uncharged reaction intermediates (e.g., fluorotelomer alcohols), sorption of PFAS to the reactor walls, and/or adsorption of F<sup>-</sup> to BOHP could also have contributed to the missing F<sup>-</sup> fraction and some overestimation of mineralization, as proposed in other works.<sup>27–29</sup>

A mechanistic explanation of the strong photocatalytic activity of BOHP in degrading PFOA will be the focus of future investigation; however, the data presented here offer some immediate insight. Reaction of hydroxyl radicals with PFOA is very slow,<sup>30</sup> and a direct mechanism involving heterogeneous reaction of PFOA with BOHP h<sub>vb</sub><sup>+</sup> and/or e<sub>cb</sub><sup>-</sup> is instead expected. As described above, the surface area, E<sub>g</sub>, and phenol oxidative degradation ability of BOHP particles under UVC irradiation were all considerably lower than those of BiPO<sub>4</sub>. Figure 3B also shows the calculated band edge potentials of catalysts studied herein, estimated using the optical band gap and geometric mean of the constituent element electronegativities according to Butler and Ginley.<sup>31</sup>

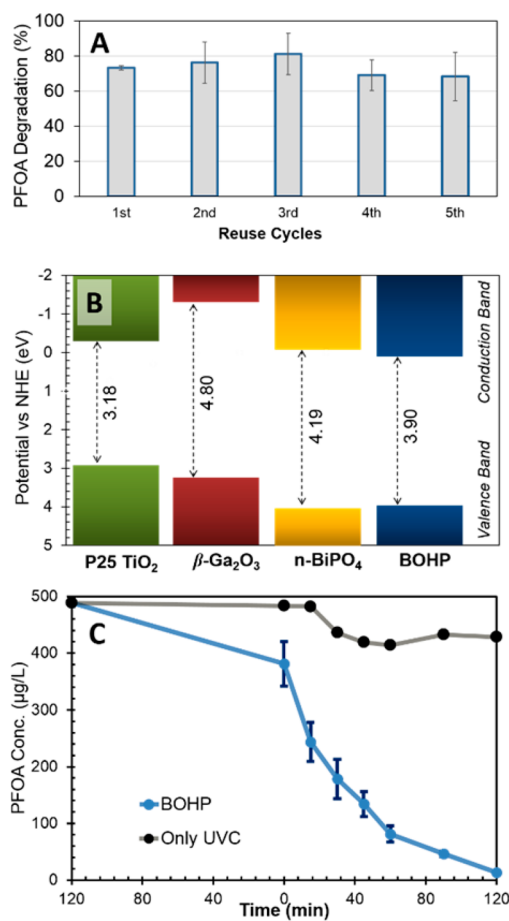


**Figure 3.** (A) Results of BOHP reusability tests showing five cycles of PFOA photocatalytic degradation in a cuvette photoreactor. Error bars show standard deviations among three parallel experiments using separately prepared BOHP batches. (B) Band gap energies and band edge potentials (estimated) of semiconductor catalysts. (C) PFOA adsorption and photocatalytic degradation by BOHP at a low initial concentration in the presence of NOM (DOC = 0.5 mg/L; pH 4; UV lamps initiated at time zero; error bars show standard deviations of triplicate experiments).

Compared to those of BiPO<sub>4</sub>, the conduction and valence band edges of BOHP are predicted to have slightly poorer redox ability (more and less positive reduction potential, respectively). It follows then that the effectiveness of BOHP in degrading PFOA and related intermediate products is not a result of the especially strong reactivity of its charge carriers, at least in comparison to that of BiPO<sub>4</sub>.

The discrepancy between phenol and PFOA activity could instead be explained by a favorable adsorption of deprotonated perfluorocarboxylic acids (PFCAs) to the hydroxylated BOHP surface resulting in stronger attraction. Feng et al. similarly found that the perfluorosulfonic acid (PFSA) adsorption capacity of iron oxides was significantly greater for hydroxylated crystal surfaces due to F...H hydrogen bonding.<sup>32</sup> Such effects may be especially pronounced considering the smaller surface area of the BOHP particles relative to the BiPO<sub>4</sub> or Ga<sub>2</sub>O<sub>3</sub> samples. With an increase in the pH of the PFOA solution to 6.2 from the natural value of ~4 upon addition of NaOH, the photocatalytic degradation rate decreased markedly and activity of BOHP became negligible at circumneutral pH (Figure S5). With a pK<sub>a</sub> of approximately 0,<sup>33,34</sup> PFOA was fully in the deprotonated form even at a pH

of 4; therefore, the greater photocatalytic efficiency under acidic conditions could instead pertain to more positively charged BOHP surfaces, resulting in electrostatic attraction of CF<sub>3</sub>(CF<sub>2</sub>)<sub>x</sub>COO<sup>-</sup>. To confirm, the BOHP particle  $\zeta$  potentials were measured at a naturally resulting suspension pH in pure water (8.45) and after adjusting to pH 4.0 using HCl, with results of -19.42 and 32.4 mV, respectively. More negative surface charge was observed for BiPO<sub>4</sub>, with  $\zeta$  potentials of -36.6 (pH 8.22) and 8.30 mV (pH 4.0). The more positively charged surface of the oxyhydroxyphosphate particles likely contributed to its faster photocatalytic PFOA degradation compared to that of BiPO<sub>4</sub>. To further confirm, adsorption experiments were performed (Text S6), using initial solution pH values of 4, 5, 6, and 7 and the same BOHP and initial PFOA concentrations that were used in photocatalysis experiments (see the Supporting Information). Results showed that the percent of PFOA (deprotonated) adsorbed to BOHP at equilibrium increased significantly with a decrease in equilibrium pH, with nearly 3 times more adsorbed at pH 4.0 than at pH 6.4, as shown in Figure S6. Moreover, BOHP's poorer activity toward phenol may also be related to electrostatic interactions, as phenol is a much weaker acid (pK<sub>a</sub> = 10.0) and the neutral protonated form was dominant in our photocatalysis experiments.

Numerous constituents of real water matrices are known to act as quenching agents in advanced oxidation processes, with carbonate species and natural organic matter (NOM) typically of greatest concern. Because of the modest pumping rates associated with groundwater treatment installations, acidification for alkalinity removal is feasible (and required in this case for the optimum pH); however, the presence of NOM during photocatalysis is less avoidable, with groundwater concentrations usually comparable to PFAS concentrations at sites contaminated by firefighting foams (10<sup>1</sup>–10<sup>2</sup>  $\mu$ g/L).<sup>35</sup> As a quick check of BOHP's susceptibility to quenching by humic substances, we conducted photocatalysis tests using prepared water with a typical groundwater DOC concentration of 500  $\mu$ g/L, the same initial PFOA concentration (1.2  $\times$  10<sup>-6</sup> M PFOA), and an initial pH of 4 (Text S4). The results in Figure 3C show that despite the lower initial concentration and the presence of NOM, PFOA was still readily degraded by BOHP, though at a slower rate (1.5 h<sup>-1</sup>) compared to that at a higher initial concentration without NOM (6.0 h<sup>-1</sup>). We note that BOHP under these conditions still outperformed the kinetics of BiPO<sub>4</sub> and reference catalysts in the pure water tests. The high affinity of PFOA for the catalyst surface may have partially counteracted the quenching by the more readily oxidized humic substances. Also, the low activity of BOHP toward phenol suggests the possibility of selectivity toward PFCAs over weakly acidic and neutral organic compounds, including NOM at this pH. A more thorough future study of the effects of complex water matrices on PFAS degradation by BOHP is warranted.

The practical limitations of photocatalytic materials and heterogeneous process reactor design were recently scrutinized by our group,<sup>36</sup> and the merits of the newly discovered BOHP photocatalyst may also be discussed in this context. As mentioned previously, small-scale slurry-type UV photocatalytic systems have seen success in industry for *ex situ* groundwater remediation and rely on highly turbulent photoreactors and membrane-based recovery of catalyst particles.<sup>13</sup> With their relatively large diameter and simple, robust morphology, BOHP microparticles may be ideal

candidates for such systems if remediation of PFCAs is a primary treatment goal. Most instances of PFAS groundwater contamination contain a wide array of fluorinated compounds, including both PFCAs and PFSA, among others.<sup>35</sup> Preliminary experiments in our lab, however, indicate BOHP is not effective in degrading perfluorooctanesulfonate, indicating a limitation in this respect (data not shown). Still, PFSA degradation technologies are likely cost intensive at full scale, and coexisting PFCAs at relatively high concentrations would result in competing reactions that detract from the PFSA degradation efficiency. Sequential schemes may therefore prove to be useful, wherein PFCAs and other organics are first degraded via a less intensive process to increase the efficiency of subsequent treatments targeting PFSA.

## ■ ASSOCIATED CONTENT

### Supporting Information

The Supporting Information is available free of charge on the ACS Publications website at DOI: 10.1021/acs.estlett.8b00395.

Details of experimental methods, BiPO<sub>4</sub> and Ga<sub>2</sub>O<sub>3</sub> XRD patterns, EDS spectra of BiPO<sub>4</sub> and BOHP, SEM image of β-Ga<sub>2</sub>O<sub>3</sub>, TOC reduction data, PFOA degradation at elevated pH, and PFOA/BOHP adsorption as a function of pH (PDF)

## ■ AUTHOR INFORMATION

### Corresponding Author

\*E-mail: [ecates@clermson.edu](mailto:ecates@clermson.edu). Phone: 864-656-1540.

### ORCID

Mohamed Ateia: 0000-0002-3524-5513

Ezra L. Cates: 0000-0003-0793-0246

### Notes

The authors declare no competing financial interest.

## ■ ACKNOWLEDGMENTS

The authors gratefully acknowledge Dr. Colin McMillen for assisting in phase identification of XRD patterns and Dr. Nishanth Tharayil for liquid chromatography–tandem mass spectrometry analyses. The authors also thank Dr. Tanju Karanfil for providing support and resources for this work.

## ■ REFERENCES

- (1) Casal, P.; González-Gaya, B.; Zhang, Y.; Reardon, A. J. F.; Martin, J. W.; Jiménez, B.; Dachs, J. Accumulation of perfluoroalkylated substances in oceanic plankton. *Environ. Sci. Technol.* **2017**, *51* (5), 2766–2775.
- (2) D'Agostino, L. A.; Mabury, S. A. Certain perfluoroalkyl and polyfluoroalkyl substances associated with aqueous film forming foam are widespread in Canadian surface waters. *Environ. Sci. Technol.* **2017**, *51* (23), 13603–13613.
- (3) Sun, M.; Arevalo, E.; Strynar, M.; Lindstrom, A.; Richardson, M.; Kearns, B.; Pickett, A.; Smith, C.; Knappe, D. R. U. Legacy and emerging perfluoroalkyl substances are important drinking water contaminants in the Cape Fear river watershed of North Carolina. *Environ. Sci. Technol. Lett.* **2016**, *3* (12), 415–419.
- (4) Appleman, T. D.; Higgins, C. P.; Quiñones, O.; Vanderford, B. J.; Kolstad, C.; Zeigler-Holady, J. C.; Dickenson, E. R. V. Treatment of poly- and perfluoroalkyl substances in U.S. full-scale water treatment systems. *Water Res.* **2014**, *51*, 246–255.
- (5) Yu, J.; Lv, L.; Lan, P.; Zhang, S.; Pan, B.; Zhang, W. Effect of effluent organic matter on the adsorption of perfluorinated

compounds onto activated carbon. *J. Hazard. Mater.* **2012**, *225–226*, 99–106.

(6) Gu, Y.; Dong, W.; Luo, C.; Liu, T. Efficient reductive decomposition of perfluorooctanesulfonate in a high photon flux UV/sulfite system. *Environ. Sci. Technol.* **2016**, *50* (19), 10554–10561.

(7) Song, Z.; Tang, H.; Wang, N.; Zhu, L. Reductive defluorination of perfluorooctanoic acid by hydrated electrons in a sulfite-mediated UV photochemical system. *J. Hazard. Mater.* **2013**, *262*, 332–338.

(8) Niu, J.; Lin, H.; Xu, J.; Wu, H.; Li, Y. Electrochemical mineralization of perfluorocarboxylic acids (PFCAs) by Ce-doped modified porous nanocrystalline PbO<sub>2</sub> film electrode. *Environ. Sci. Technol.* **2012**, *46* (18), 10191–10198.

(9) Niu, J.; Li, Y.; Shang, E.; Xu, Z.; Liu, J. Electrochemical oxidation of perfluorinated compounds in water. *Chemosphere* **2016**, *146*, 526–538.

(10) Zhao, B.; Li, X.; Yang, L.; Wang, F.; Li, J.; Xia, W.; Li, W.; Zhou, L.; Zhao, C. β-Ga<sub>2</sub>O<sub>3</sub> nanorod synthesis with a one-step microwave irradiation hydrothermal method and its efficient photocatalytic degradation of perfluorooctanoic acid. *Photochem. Photobiol.* **2015**, *91* (1), 42–47.

(11) Zhao, B.; Lv, M.; Zhou, L. Photocatalytic degradation of perfluorooctanoic acid with β-Ga<sub>2</sub>O<sub>3</sub> in anoxic aqueous solution. *J. Environ. Sci.* **2012**, *24* (4), 774–780.

(12) Zhao, B.; Zhang, P. Photocatalytic decomposition of perfluorooctanoic acid with β-Ga<sub>2</sub>O<sub>3</sub> wide bandgap photocatalyst. *Catal. Commun.* **2009**, *10* (8), 1184–1187.

(13) Benotti, M. J.; Stanford, B. D.; Wert, E. C.; Snyder, S. A. Evaluation of a photocatalytic reactor membrane pilot system for the removal of pharmaceuticals and endocrine disrupting compounds from water. *Water Res.* **2009**, *43* (6), 1513–1522.

(14) Shao, T.; Zhang, P.; Jin, L.; Li, Z. Photocatalytic decomposition of perfluorooctanoic acid in pure water and sewage water by nanostructured gallium oxide. *Appl. Catal., B* **2013**, *142–143*, 654–661.

(15) Xu, Y.; Schoonen, M. A. A. The absolute energy positions of conduction and valence bands of selected semiconducting minerals. *Am. Mineral.* **2000**, *85*, 543.

(16) Huang, D.; Yin, L.; Lu, X.; Lin, S.; Niu, Z.; Niu, J. Directional electron transfer mechanisms with graphene quantum dots as the electron donor for photodecomposition of perfluorooctane sulfonate. *Chem. Eng. J.* **2017**, *323*, 406–414.

(17) Pan, C.; Zhu, Y. New Type of BiPO<sub>4</sub> oxy-acid salt photocatalyst with high photocatalytic activity on degradation of dye. *Environ. Sci. Technol.* **2010**, *44* (14), 5570–5574.

(18) Tian, X.; Xu, T.; Wang, Y.; Meng, S. Hierarchical h-, m- and n-BiPO<sub>4</sub> microspheres: Facile synthesis and application in the photocatalytic decomposition of refractory phenols and benzene. *RSC Adv.* **2017**, *7* (58), 36705–36713.

(19) Pan, C.; Li, D.; Ma, X.; Chen, Y.; Zhu, Y. Effects of distortion of PO<sub>4</sub> tetrahedron on the photocatalytic performances of BiPO<sub>4</sub>. *Catal. Sci. Technol.* **2011**, *1* (8), 1399–1405.

(20) Pan, C.; Zhu, Y. A review of BiPO<sub>4</sub>, a highly efficient oxyacid-type photocatalyst, used for environmental applications. *Catal. Sci. Technol.* **2015**, *5* (6), 3071–3083.

(21) Krause, W.; Belendorff, K.; Bernhardt, H. J. Petitjeanite, Bi<sub>3</sub>O(OH)(PO<sub>4</sub>)<sub>2</sub>, a new mineral, and additional data for the corresponding arsenate and vanadate, preisingerite and schumacherite. *Neues Jahrb. Mineral., Monatsh.* **1993**, 487–503.

(22) Sahu, S. P.; Cates, E. L. X-ray radiocatalytic activity and mechanisms of bismuth complex oxides. *J. Phys. Chem. C* **2017**, *121* (19), 10538–10545.

(23) Bedliwy, D.; Mereiter, K. Preisingerite, Bi<sub>3</sub>O(OH)(AsO<sub>4</sub>)<sub>2</sub>, a new species from San Juan Province, Argentina: Its description and crystal structure. *Am. Mineral.* **1982**, *67*, 833–840.

(24) Lv, Y.; Zhu, Y.; Zhu, Y. Enhanced photocatalytic performance for the BiPO<sub>4-x</sub> nanorod induced by surface oxygen vacancy. *J. Phys. Chem. C* **2013**, *117* (36), 18520–18528.

(25) Medvedeva, N. I.; Zhukov, V. P.; Gubanov, V. A.; Novikov, D. L.; Klein, B. M. Electronic structure and chemical bonding in  $\delta$ -Bi<sub>2</sub>O<sub>3</sub>. *J. Phys. Chem. Solids* **1996**, *57* (9), 1243–1250.

(26) Benskin, J. P.; De Silva, A. O.; Martin, J. W. Isomer profiling of perfluorinated substances as a tool for source tracking: A review of early findings and future applications. In *Reviews of Environmental Contamination and Toxicology Vol. 208: Perfluorinated alkylated substances*; De Voogt, P., Ed.; Springer: New York, 2010; pp 111–160.

(27) Sun, B.; Ma, J.; Sedlak, D. L. Chemisorption of perfluorooctanoic acid on powdered activated carbon initiated by persulfate in aqueous solution. *Environ. Sci. Technol.* **2016**, *50* (14), 7618–7624.

(28) van Leeuwen, S. P. J.; de Boer, J. Extraction and clean-up strategies for the analysis of poly- and perfluoroalkyl substances in environmental and human matrices. *J. Chromatogr. A* **2007**, *1153* (1), 172–185.

(29) Bruton, T. A.; Sedlak, D. L. Treatment of aqueous film-forming foam by heat-activated persulfate under conditions representative of in situ chemical oxidation. *Environ. Sci. Technol.* **2017**, *51* (23), 13878–13885.

(30) Hori, H.; Hayakawa, E.; Einaga, H.; Kutsuna, S.; Koike, K.; Ibusuki, T.; Kiatagawa, H.; Arakawa, R. Decomposition of environmentally persistent perfluorooctanoic acid in water by photochemical approaches. *Environ. Sci. Technol.* **2004**, *38* (22), 6118–6124.

(31) Butler, M. A.; Ginley, D. S. Prediction of flatband potentials at semiconductor-electrolyte interfaces from atomic electronegativities. *J. Electrochem. Soc.* **1978**, *125* (2), 228–232.

(32) Feng, H.; Lin, Y.; Sun, Y.; Cao, H.; Fu, J.; Gao, K.; Zhang, A. In silico approach to investigating the adsorption mechanisms of short chain perfluorinated sulfonic acids and perfluorooctane sulfonic acid on hydrated hematite surface. *Water Res.* **2017**, *114*, 144–150.

(33) Goss, K.-U. The pK<sub>a</sub> values of PFOA and other highly fluorinated carboxylic Acids. *Environ. Sci. Technol.* **2008**, *42* (2), 456–458.

(34) Cheng, J.; Psillakis, E.; Hoffmann, M. R.; Colussi, A. J. Acid dissociation versus molecular association of perfluoroalkyl oxoacids: Environmental implications. *J. Phys. Chem. A* **2009**, *113* (29), 8152–8156.

(35) Backe, W. J.; Day, T. C.; Field, J. A. Zwitterionic, cationic, and anionic fluorinated chemicals in aqueous film forming foam formulations and groundwater from U.S. military bases by non-aqueous large-volume injection HPLC-MS/MS. *Environ. Sci. Technol.* **2013**, *47* (10), 5226–5234.

(36) Cates, E. L. Photocatalytic water treatment: So where are we going with this? *Environ. Sci. Technol.* **2017**, *51* (2), 757–758.